Formation of tropical anvil clouds by slow evaporation

Jacob T. Seeley[1], Nadir Jeevanjee[2,3], Wolfgang Langhans[4], and David M. Romps[1,4]

[1]Department of Earth and Planetary Science, University of California, Berkeley, CA 94720
[2]Department of Geosciences, Princeton University, Princeton, NJ 08544
[3]Geophysical Fluid Dynamics Laboratory, Princeton, NJ 08540
[4]Climate and Ecosystem Sciences Division, Lawrence Berkeley National Laboratory, Berkeley, CA 94720

Key Points:

- The sources and sinks of cloudy air are quantified and manipulated in cloud-resolving simulations of radiative-convective equilibrium
- The cloud-fraction peak associated with anvil clouds is found to result from the long lifetime of cloud condensates in the upper troposphere
- Cloud lifetimes are long in the upper troposphere due to the slow evaporation of cloud condensates at cold temperatures

Corresponding author: Jacob T. Seeley, jacob.t.seeley@gmail.com

Abstract

Tropical anvil clouds play a large role in Earth's radiation balance, but their effect on global warming is uncertain. The conventional paradigm for these clouds attributes their existence to the rapidly-declining convective mass flux below the tropopause, which implies a large source of detraining cloudy air there. Here, we test this paradigm by manipulating the sources and sinks of cloudy air in cloud-resolving simulations. We find that anvils form in our simulations because of the long lifetime of upper-tropospheric cloud condensates, not because of an enhanced source of cloudy air below the tropopause. We further show that cloud lifetimes are long in the cold upper troposphere because the saturation specific humidity is much smaller there than the condensed water loading of cloudy updrafts, which causes evaporative cloud decay to act very slowly. Our results highlight the need for novel cloud-fraction schemes that align with this decay-centric framework for anvil clouds.

1 Introduction

The upper tropical troposphere is one of the cloudiest places on Earth (Figure 1). The production of this abundant high cloud can be observed during the life cycle of a single cumulonimbus: the cloudiness reaches the greatest radius in the upper troposphere, causing the cumulonimbus to resemble a blacksmith's anvil. For this reason, the extensive high clouds are referred to as anvil clouds.

Tropical anvil clouds play a large role in Earth's radiation balance by reflecting sunlight and throttling the flow of terrestrial radiation to space (Boucher et al., 2013; D. L. Hartmann, Moy, & Fu, 2001). However, the effect of anvil clouds on anthropogenic global warming is uncertain. One suggestion — known as the iris hypothesis — posits that anvil clouds shrink as the surface warms, thereby acting as a negative feedback on warming by allowing the surface to more easily emit radiation to space (D. L. Hartmann & Michelsen, 2002; B. Lin, Wielicki, Chambers, Hu, & Xu, 2002; Lindzen, Chou, & Hou, 2001; Mauritsen & Stevens, 2015). Another idea is the Fixed Anvil Temperature (FAT) hypothesis, which proposes that anvil clouds will rise with warming so as to remain at a fixed temperature, thereby acting as a positive feedback (D. Hartmann & Larson, 2002; Kuang & Hartmann, 2007). Before we can assess these and any other potential anvil-radiative feedbacks, we must first understand the basic physical processes that produce anvil clouds.

The central question addressed here is: Why do cumulonimbus clouds resemble anvils? Or, phrased another way, why does tropical cloud fraction peak in the upper troposphere? One potential explanation is that tropospheric radiative cooling decreases to zero at the tropopause. Since convective heating is required to balance this radiative cooling, clouds must rise through most of the troposphere and then cease rising in the upper troposphere. As the argument goes, the pileup of mass as the clouds come to a halt causes the cloudy air to spread out laterally, forming the peak in cloud fraction below the tropopause. This explanation for anvil clouds has become the conventional view (Boucher et al., 2013). This paradigm is typically described in terms of clear-sky convergence (Bony et al., 2016; Harrop & Hartmann, 2012; D. Hartmann & Larson, 2002; D. L. Hartmann, 2016; Kuang & Hartmann, 2007; Kubar, Hartmann, & Wood, 2007; Li, Yang, North, & Dessler, 2012; Thompson, Bony, & Li, 2017; Zelinka & Hartmann, 2010, 2011), and is formalized mathematically by:

$$\mathcal{C} = \max\left(0, -\frac{1}{\rho}\frac{\partial M}{\partial z}\right)\tau_0. \tag{1}$$

Here, $\mathcal{C}$ is the cloud fraction, M is the convective mass flux (units of kg/m^2/s), and τ_0 is a constant timescale (units of s) that quantifies the lifetime of cloudy air. Since τ_0 is independent of height, cloud sinks play no role in shaping the cloud-fraction

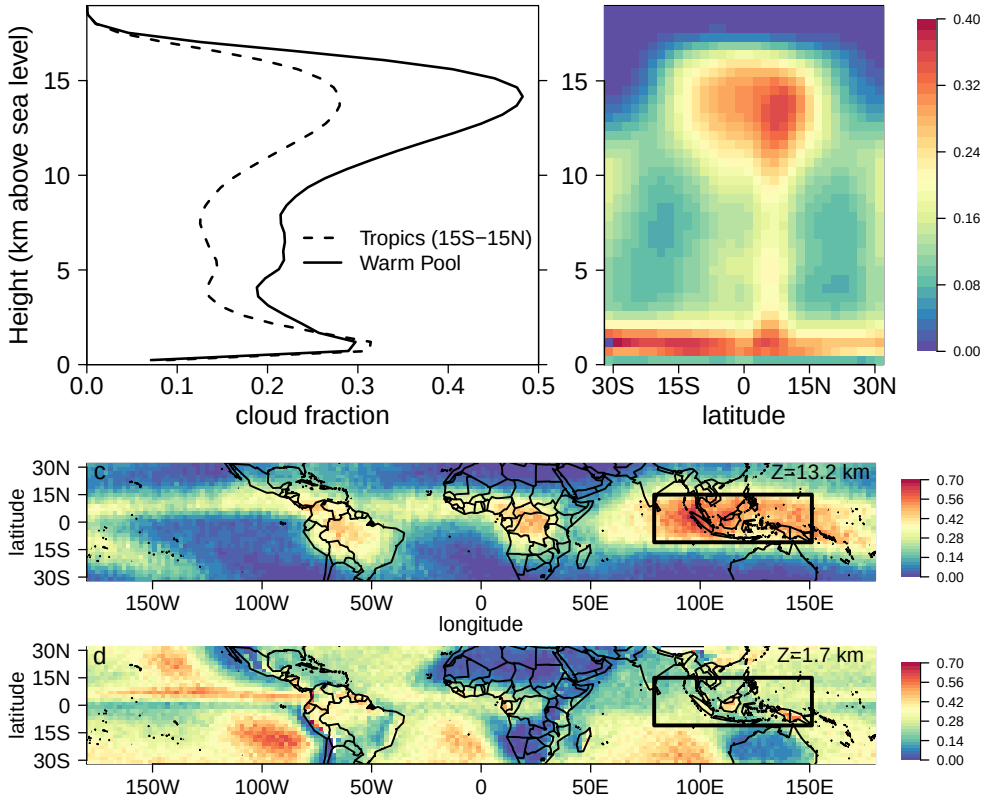

Figure 1. Cloud fraction from colocated spaceborne radar (CloudSat) and lidar (Cloud-Aerosol LIdar with Orthogonal Polarization; CALIOP) as described in Kay and Gettelman (2009). The data are averaged over 07/2006–02/2011 and plotted (a) as a function of altitude; (b) as a function of latitude and altitude (zonal average); as a function of latitude and longitude at (c) an altitude of 13.2 km and (d) an altitude of 1.7 km. In (a), the cloud fraction for the Indo-Pacific "Warm Pool" is obtained by averaging within the black boxes in panels (c) and (d). In (d), grid cells with surface topography higher than 1.7 km are left blank.

profile predicted by this clear-sky convergence (CSC) paradigm. According to the CSC paradigm, $\mathcal{C}$ maximizes in the upper troposphere because that is where clear-sky convergence, equal to $-(1/\rho)\partial M/\partial z$, is greatest.

2 Testing the clear-sky convergence paradigm

To assess the CSC paradigm, we use cloud-resolving simulations of tropical convection in radiative-convective equilibrium (RCE), which are well-suited to studying anvil clouds (Harrop & Hartmann, 2012, 2016; Kuang & Hartmann, 2007). We begin by examining the DEFAULT simulation, which is run at relatively high resolution, includes cloud-radiative interactions, and uses a realistic microphysics scheme that accounts for ice processes (Table 1). Further simulation details are provided in *Text S1*.

experiment	Δx	Δz	Δt	**microphysics**	**radiation**
DEFAULT	200 m	100 m	5 s	LLK	all-sky RRTM
DEFAULT_CLR	200 m	100 m	5 s	LLK	clear-sky RRTM
CTRL	2 km	250 m	20 s	simple	clear-sky RRTM
NOEVAP	2 km	250 m	20 s	simple, no evap.	prescribed
NOPEAK	2 km	250 m	20 s	simple	prescribed
LOPEAK	2 km	250 m	20 s	simple	prescribed

Table 1. Experiment configurations with the cloud-resolving model DAM (Romps, 2008). Δz refers to the free-tropospheric vertical grid spacing. "LLK" microphysics refers to DAM's default Lin-Lord-Krueger scheme (Krueger et al., 1995; Y.-L. Lin et al., 1983; Lord et al., 1984). The "simple" microphysics is a Kessler-type scheme based on an autoconversion timescale (Kessler, 1969) described in more detail in the main text. Simulations with non-prescribed radiative cooling profiles used the Rapid Radiative Transfer Model (RRTM; Clough et al., 2005; Iacono et al., 2008).

Figure 2a shows the CSC paradigm's predictions for the DEFAULT simulation. This paradigm predicts an anvil peak in approximately the right location, but also predicts the largest overall cloud fraction in the lower troposphere, which disagrees with the simulation, and predicts an additional prominent mid-tropospheric peak in cloud fraction that does not exist in the CRM. Although the CSC literature has not explicitly attempted to understand mid- or low-level cloud fraction in terms of clear-sky convergence, neither has this literature argued that the CSC mechanism only functions in the upper troposphere. The mismatch between clear-sky convergence and cloud fraction in the mid- and lower-troposphere of DEFAULT suggests that we should interrogate the assumptions of the CSC paradigm.

The faulty predictions of the CSC paradigm in the mid- and lower-troposphere can be traced back to two potential sources of error. First, since cloudy updrafts entrain clear air as they rise through the troposphere, clear-sky convergence only puts a lower bound on the correct source term for cloudy air (e.g., Yanai, Esbensen, & Chu, 1973). The correct source is the volumetric detrainment of cloud, $D/\rho = \delta M/\rho$, where δ (m^{-1}) is the bulk-plume fractional detrainment rate. The use of net detrainment (i.e., clear-sky convergence) instead of gross detrainment may give a misleading impression of where in the troposphere cloud sources are largest.

The second potential source of error is that cloud lifetimes may not be independent of height, as the CSC paradigm assumes. To assess the validity of the constant-lifetime assumption, we first used the water budget to diagnose the volumetric detrainment in the DEFAULT simulation. Cloudy grid cells were identified as those in which $q_c \geq 10^{-5}$ kg/kg, where q_c is the mass fraction of non-precipitating cloud condensate (this threshold was adopted from previous work, e.g. Kuang and Hartmann (2007)). We further divided cloudy air into "updraft" and "inactive" categories with a vertical velocity threshold (*Text S1*). Denoting the mean condensate loading of cloudy updrafts as q_{c0}, the evaporation/sublimation rate as e and the conversion rate of cloud condensate to precipitating water as p (both with units of $\mathrm{kg/m^3/s}$, averaged in time and over all non-updraft cloudy grid cells), the steady-state cloud-water budget for inactive air is

$$\delta M q_{c0} = e + p. \tag{2}$$

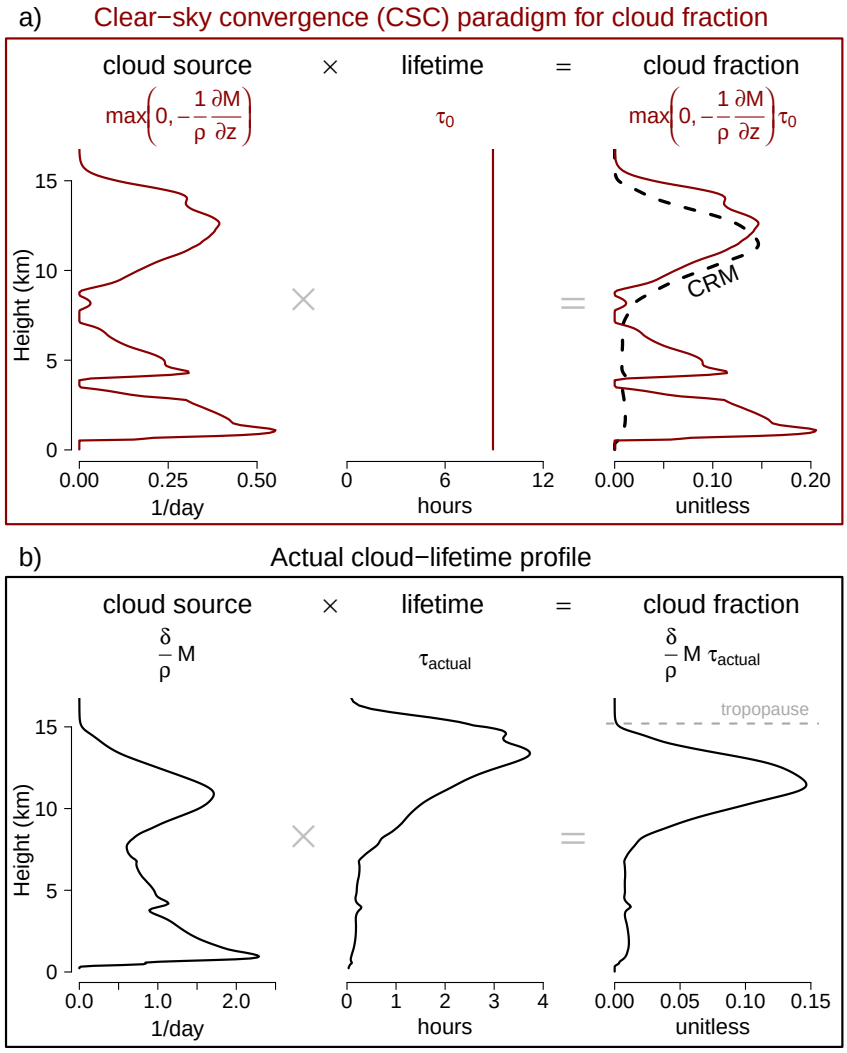

Figure 2. (a) The three columns inside the dark red box show how the CSC paradigm predicts cloud fraction: by taking the product of a source term (clear-sky convergence) and a vertically-uniform timescale, τ_0 (set here to 8.9 hours to obtain the best fit with the magnitude of upper-tropospheric cloud fraction). The dotted black line in the third column shows the actual time-mean cloud fraction from the CRM experiment (with the contribution from updrafts removed). (b) The three columns inside the black box show how the correct source term (the volumetric detrainment) multiplied by the actual cloud-lifetime profile (τ_{actual}) yields the cloud fraction. The tropopause is marked with a dashed gray line in the bottom-right panel.

We recorded profiles of M, q_{c0}, e, and p as part of the statistics from our simulations, so that all terms in equation 2 except for δ are directly measured from the simulation. This allows us to diagnose the volumetric detrainment, $\delta M/\rho$. The actual cloud-lifetime profile, τ_{actual}, can then be inferred by dividing the cloud fraction by this source term.

The results of this procedure are shown in Figure 2b. The volumetric detrainment profile in the DEFAULT simulation has a broad resemblance to the clear-sky convergence profile, but is significantly larger in magnitude and does not go to zero

except at the bottom and top of the convecting troposphere. We note that the volumetric detrainment bears little resemblance to a blacksmith's anvil: the actual source term for cloudy air maximizes in the lower troposphere, and only varies by a factor of about 3 over the bulk of the troposphere. Therefore, the source term does not explain the top-heaviness of the cloud-fraction profile in this simulation.

The inferred cloud-lifetime profile, on the other hand, is very top-heavy. Whereas τ_{actual} hovers between 5–15 minutes at altitudes below 7 km, in the upper troposphere it grows to almost 4 hours, which is an increase of more than an order of magnitude. Therefore, the increase in cloud lifetimes in the upper troposphere is fundamental to understanding why the cloud-fraction profile in this simulation resembles a blacksmith's anvil.

3 Cloud sinks shape the cloud-fraction profile

Why are cloud lifetimes so top-heavy? To answer this question, we conducted additional RCE simulations with a simplified configuration of the CRM (Table 1; *Text S1*). The most salient aspect of the simplified CRM configuration is that microphysics was treated with a Kessler-type scheme (Kessler, 1969) in order to facilitate a quantitative analysis of cloud sinks. There is no explicit ice phase in this scheme, so the only classes of water are vapor, non-precipitating cloud condensate, and precipitation (with mass fractions q_v, q_c, and q_p, respectively). Other than the condensation and evaporation that occur during saturation adjustment, the only microphysical process included in this scheme is autoconversion of cloud condensate to precipitation, which is parameterized as

$$a = -q_c/\tau_a, \tag{3}$$

where a (s^{-1}) is the sink of cloud condensate from autoconversion and τ_a (s) is an autoconversion timescale that we set to 75 minutes in inactive cloudy air. Despite its simplicity, the standard version of this simplified configuration (CTRL) reproduces the key features of the DEFAULT simulation: the anvil-shaped cloud fraction profile, the bottom-heavy source term, and the top-heavy cloud-lifetime profile (Figures S1,S2). The similarity between the DEFAULT and CTRL simulations suggests that the basic formation mechanism of anvil clouds does not involve the details of ice microphysics, despite the fact that in nature these clouds are composed of ice crystals.

To illuminate the role of cloud sinks in shaping the cloud-fraction profile, we reran the CTRL simulation with evaporation of cloud condensate artificially prevented (the NOEVAP experiment, in which precipitation is the only microphysical sink of cloud water; *Text S1*). Figure 3 shows the result: preventing evaporation of cloud condensate strongly increases cloud fraction in the lower troposphere, but has only a modest effect on cloud fraction in the upper troposphere. This stark contrast is a result of Clausius-Clapeyron: very little condensed water can evaporate into subsaturated air at cold temperatures, so precipitation already serves as the dominant pathway for cloud decay in the upper troposphere even when evaporation is turned on. (Here and throughout, we use the term "evaporation" to refer to both evaporation and sublimation, and we use "precipitation" to refer to both precipitation and sedimentation.) On the other hand, the warmer temperatures of the lower troposphere ordinarily lead to fast evaporation of detrained cloud condensate, which allows for a large increase in cloud fraction when evaporation is prevented. The NOEVAP experiment shows that if clouds at all altitudes were forced to decay in the manner of upper-tropospheric clouds — that is, by precipitating out, rather than evaporating — cloud fraction would be bottom-heavy, rather than top-heavy. This suggests that vertical variations in evaporation play a key role in the formation of anvil clouds in our simulations.

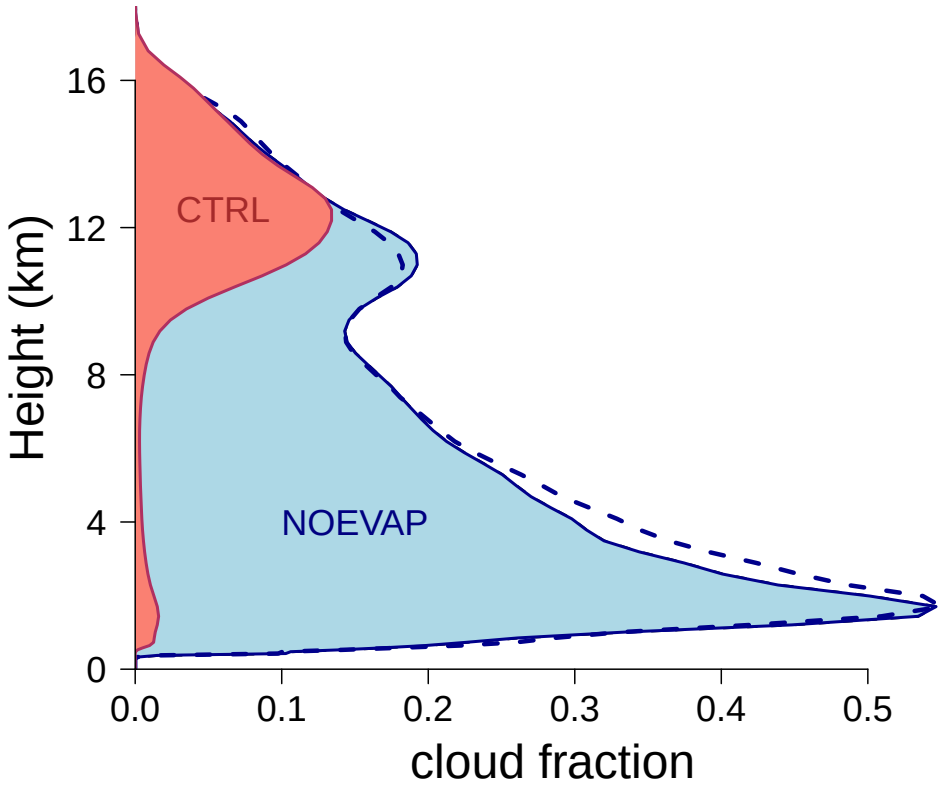

Figure 3. Cloud fraction from the CTRL and NOEVAP experiments (solid lines with colored shading). In NOEVAP, evaporation of cloud condensate is prevented while holding environmental relative humidity and detrainment fixed from CTRL as described in *Text S1*. The dashed blue line shows the cloud fraction predicted for the NOEVAP experiment by the new framework for anvil clouds. Because of the large cloud fraction in the lower troposphere of NOEVAP, the version of the new framework that accounts for cloud overlap (equation S38) is used here.

4 Analytical model of cloud decay

Since the vertically-varying sinks of cloudy air play a leading role in shaping the cloud-fraction profile in our simulations, a viable theory for anvil clouds must account for how cloud lifetimes change over the depth of the troposphere. Here we give an abbreviated derivation of an analytical model for cloud lifetimes that incorporates the physics of evaporation, dilution, and precipitation as sinks of cloud condensate; the complete derivation is given in *Text S2*.

Consider a cylindrical cloud with initial radius r_0 and constant height h. We assume the cloud is initially filled with turbulence with a uniform eddy velocity of v_0, and that the cloud's boundary r expands radially outward at a rate proportional to the cloud's internal eddy velocity v with constant of proportionality c. For a quiescent environment and in the limit of no dissipation, the cloud conserves its kinetic energy as it grows, which implies that the cloud's area A grows linearly in time:

$$A(t) = A_0 \left(1 + t/\kappa\right), \tag{4}$$

where $A_0 = \pi r_0^2$ is the cloud's initial area and $\kappa \equiv r_0/(2cv_0)$ is a constant with dimensions of time. κ can be interpreted as the amount of time it takes the cloud to grow in area by an amount equal to its initial area A_0. We treat κ as a tuning parameter (*Text S2*), which is set to 19 minutes for all figures in the main text.

To determine the lifetime of the cloud, we use its bulk water budget (i.e., the cloud's properties are assumed to be homogeneous). We will first model a cloud whose only sink of condensed water is from mixing with environmental air, and then add the effects of precipitation. Initially, the cloud has total water mass fraction $q_t = q_{c0} + q_v^*$, while the cloud's environment has total water $\mathrm{RH}q_v^*$, where RH is the environmental relative humidity and q_v^* is the saturation specific humidity. Therefore, under the influence of mixing, the cloud's q_t evolves in time according to

$$\frac{dq_t}{dt} = -\left(\frac{1}{\kappa + t}\right)\left[q_c(t) + q_v^*(1 - \mathrm{RH})\right], \tag{5}$$

where the first and second terms inside the brackets represent dilution and evaporation, respectively.

As long as the cloud is saturated, its vapor mass fraction is pegged at the saturation value q_v^*, and equation 5 is really the governing equation for the cloud's condensed water q_c. The solution is analytic, and since we define cloudy air as having $q_c \geq 10^{-5}$ kg/kg, we can set $q_c(t) = 10^{-5}$ to solve for the "mixing-only" lifetime of the cloud, $\tilde{\tau}_{\mathrm{mix}}$:

$$\tilde{\tau}_{\mathrm{mix}} = \kappa \chi_c, \tag{6}$$

where

$$\chi_c \equiv \frac{q_{c0} - 10^{-5}}{q_v^*(1 - \mathrm{RH}) + 10^{-5}}. \tag{7}$$

χ_c is a very important parameter in cloud decay physics, because it measures the efficiency with which mixing causes cloudy air to decay: if one part of cloudy air with an initial condensate loading of q_{c0} mixes with χ_c parts of environmental air with a saturation deficit of $q_v^*(1 - \mathrm{RH})$, the cloudy parcel will become clear. We will see that χ_c is key to understanding the top-heaviness of cloud-fraction profiles in our simulations.

So far, we have neglected an important sink of cloud condensates in decaying clouds: precipitation. If precipitation (parameterized by equation 3, in accordance with our simulations) were the only process causing the cloud to decay, its lifetime would be given by:

$$\tilde{\tau}_{\mathrm{precip}} = \tau_a \log\left(q_{c0}/10^{-5}\right). \tag{8}$$

Combining the effects of precipitation and mixing, then, equation 5 is modified to

$$\frac{dq_t}{dt} = -\left(\frac{1}{\kappa + t}\right)\left[q_c(t) + q_v^*(1 - \mathrm{RH})\right] - q_c(t)/\tau_a, \tag{9}$$

and the new expression for the cloud's lifetime $\tilde{\tau}_{\mathrm{new}}$ is:

$$\tilde{\tau}_{\text{new}} = \tau_a \left[W\left(ae^b\right) - b \right]; \tag{10a}$$

$$a = \frac{\kappa}{\tau_a}\left(\frac{q_{c0}}{10^{-5}}\right) + \frac{q_v^*(1-\text{RH})}{10^{-5}}; \tag{10b}$$

$$b = \frac{\kappa}{\tau_a} + \frac{q_v^*(1-\text{RH})}{10^{-5}}, \tag{10c}$$

where W is the Lambert W function.

For cloud fraction, what matters is not just the lifetime of the decaying cloud but its time-integrated area. Therefore, it is convenient to define an "effective lifetime", τ, such that a cloud that has constant area of A_0 during a lifetime of length τ would produce the same time-integrated cloud fraction as one that grows for a lifetime of $\tilde{\tau}$ as it decays:

$$\tau = \int_0^{\tilde{\tau}} \frac{A(t)}{A_0}\, dt. \tag{11}$$

For mixing-induced decay, the effective lifetime is therefore

$$\tau_{\text{mix}} = \kappa\left(\chi_c + \frac{\chi_c^2}{2}\right). \tag{12}$$

The effective lifetime for precipitation-only decay is already given by equation 8 since such a cloud decays in place, while the effective lifetime for mixing and precipitation combined is

$$\tau_{\text{new}} = \tilde{\tau}_{\text{new}} + \frac{\tilde{\tau}_{\text{new}}^2}{2\kappa}. \tag{13}$$

Equation 13, with $\tilde{\tau}_{\text{new}}$ given by equations 10, is an analytical expression for the effective lifetime of a cloud as a function of its initial condensed water q_{c0}, environmental saturation deficit $q_v^*(1-\text{RH})$, mixing timescale κ, and precipitation timescale τ_a.

5 Cloud lifetimes are top-heavy due to slow evaporation

The analytical model of cloud decay presented in the previous section allows us to understand why cloud lifetimes are top-heavy. In Figure 4a, we plot χ_c from the CTRL experiment. In the lower troposphere, $\chi_c < 1$, and mixing easily evaporates cloudy air. In the upper troposphere, however, the updraft-mean condensate loading q_{c0} becomes much larger than the environmental saturation deficit $q_v^*(1-\text{RH})$, and $\chi_c \gg 1$. This mismatch between the amount of condensed water delivered by clouds and the ability of the environment to absorb it can occur because updraft condensate loading is not constrained by the local environmental temperature — unlike the saturation deficit, which must decline exponentially with decreasing temperature due to Clausius-Clapeyron. As a consequence, when upper-tropospheric clouds mix with environmental air, they can easily bring that environmental air to saturation with plenty of cloud condensate to spare. This greatly enhances the time-integrated area of decaying clouds in the upper troposphere.

Although the saturation deficit is given by $q_v^*(1-\text{RH})$, it is important to note that the profile of χ_c is driven by q_v^*, not vertical variations in RH. The dashed curve in Figure 4a shows χ_c calculated with RH set to its tropospheric mean. Clearly, the growth in χ_c with height is caused by the rapid exponential decay of q_v^*, not the relatively high RH of the upper troposphere.

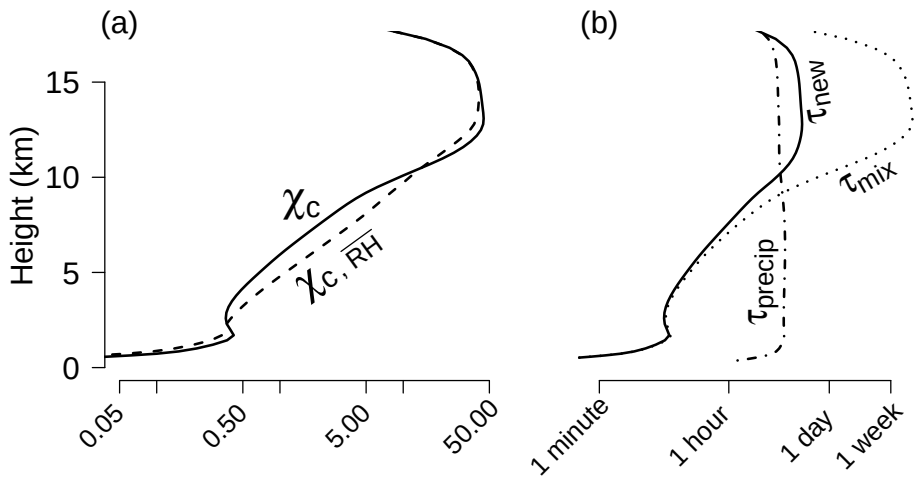

Figure 4. (a) The profile of χ_c from the CTRL experiment (eqn. 7). χ_c gives the number of parts of environmental air with which one part of cloudy air must mix in order to become clear. The dashed line shows χ_c calculated with relative humidity (RH) set to its tropospheric-mean, $\overline{\text{RH}}$. (b) From the CTRL experiment, effective cloud lifetimes from mixing and precipitation considered individually (τ_{mix} and τ_{precip}, eqns. 12 and 8) and in combination (τ_{new}, equation 13).

The efficiency of mixing-induced decay is a key determinant of a cloud's lifetime. In Figure 4b, we plot the effective cloud lifetime from mixing alone, τ_{mix}. Because of the dependence of τ_{mix} on χ_c (equation 12), effective cloud lifetimes due to mixing are extremely top-heavy, ranging from only a few minutes in the lower troposphere to over 1 week in the upper troposphere. Also plotted in Figure 4b is the effective cloud lifetime due to precipitation alone, τ_{precip} (equation 8). Unlike the top-heavy τ_{mix}, τ_{precip} is roughly constant throughout the bulk of the troposphere.

The analytical expression for τ_{new} (equation 13) combines the physics of mixing and precipitation. Therefore, τ_{new} is driven to large values in the upper troposphere by the ballooning of τ_{mix} (Figure 4b). Note, however, that the largest upper-tropospheric values of τ_{mix} significantly exceed τ_{new} there, because actual cloud lifetimes are limited by precipitation even in the limit of no evaporation. Indeed, Figure 4 shows that the decay pathway for clouds transitions from a fast, mixing-dominated regime in the lower troposphere ($\tau_{\text{new}} \simeq \tau_{\text{mix}}$) to a slower, precipitation-dominated regime in the upper troposphere ($\tau_{\text{new}} \simeq \tau_{\text{precip}}$). This is further confirmed by comparing the microphysical sinks of cloud condensate averaged over decaying clouds: in both DEFAULT and CTRL, evaporation far outweighs precipitation as a sink in the lower troposphere, whereas precipitation dominates at the anvil level (Figure S3). Although the analytical model is highly idealized, results from a more complex model of cloud decay that numerically solves the diffusion equation are nearly identical to the analytical theory (*Text S3*; Figure S9).

6 A new framework for anvil clouds

Putting the correct source term for cloudy air together with the effective lifetime predicted by equation 13 yields the "new framework" for anvil clouds:

$$\mathcal{C} = \frac{\delta M}{\rho} \tau_{\text{new}}. \tag{14}$$

We note that equation 14 is the first-order Taylor-expansion of a more general equation for cloud fraction that acounts for overlap between clouds (*Text S4*); in the limit of large cloud fraction, the more general equation should be used in order to prevent over-estimation.

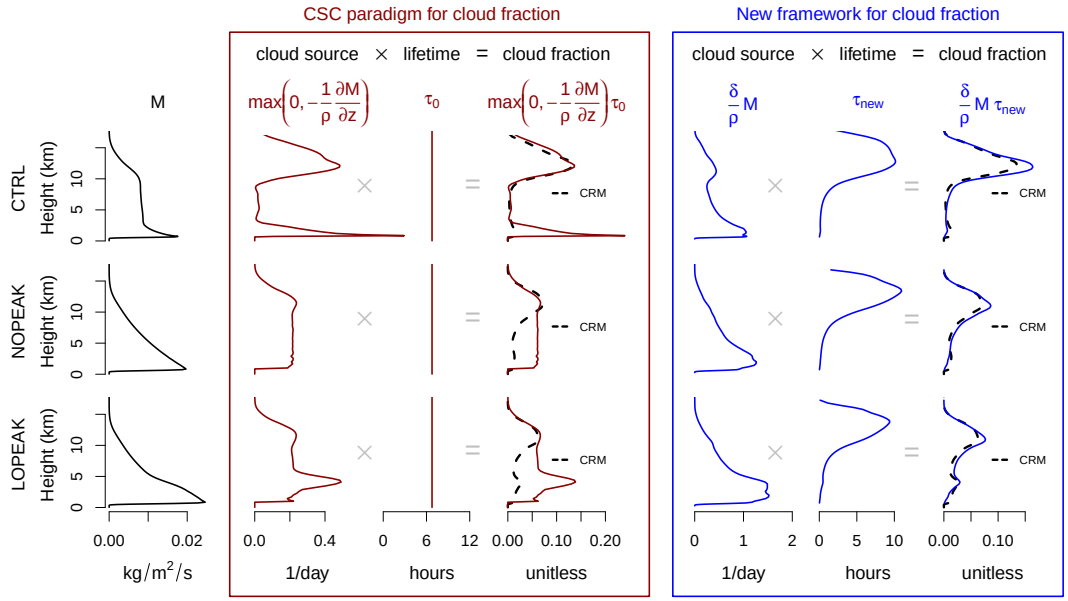

Figure 5. Comparison of the CSC paradigm and the new framework for anvil clouds (red and blue boxes, respectively). The three rows correspond to the three experiments (CTRL, NOPEAK, and LOPEAK, respectively). In each row, the first column shows the convective updraft mass flux M. The next three columns, color-coded in dark red, show how the CSC paradigm for anvil clouds predicts cloud fraction (fourth column) as the product of a source term (clear-sky convergence, second column) times a vertically-uniform timescale, τ_0 (third column). The final three columns, color-coded in blue, likewise show how the new framework for anvil clouds predicts cloud fraction (seventh column) as the product of a source term (the volumetric detrainment, fifth column) times an analytic expression for cloud lifetime, τ_{new}, that varies with height (sixth column). The dotted black lines in the fourth and seventh columns show the actual cloud fraction from the CRM experiment (with the contribution from updrafts removed).

In the top row of Figure 5, we apply the CSC paradigm and the new framework to the CTRL experiment. As in the DEFAULT experiment, the CSC paradigm predicts the largest cloud fraction in the lower troposphere, which disagrees with the simulation. On the other hand, the new framework correctly places the anvil peak in the upper troposphere. The new framework predicts the top-heavy shape of the cloud-fraction profile even though the source term (the volumetric detrainment, again diagnosed from the water budget by equation 2) maximizes in the lower troposphere. It is the ballooning of cloud lifetimes in the upper troposphere — which is predicted by the analytical expression for τ_{new} — that causes the large peak in cloud fraction there in the CTRL experiment.

When cloud evaporation is prevented, as in the NOEVAP experiment, this ballooning of upper-tropospheric cloud lifetimes is eliminated. With no retuning of parameters, the new framework accurately predicts the bottom-heavy cloud-fraction profile of the NOEVAP experiment (dashed blue line, Figure 3; in the new framework, evaporation is prevented by setting the environmental RH to 1 in eqns. 10). Without fast evaporation of condensates in the lower troposphere, cloud lifetimes only vary by a factor of about 2 over the bulk of the troposphere (Figure S9b). This causes cloud fraction to peak in the lower troposphere, where there is the most detrainment.

Figure 5 also shows results from two experiments in which the radiative-cooling profiles were modified to produce different clear-sky convergence profiles (the NOPEAK and LOPEAK experiments; *Text S1*). In the NOPEAK experiment, the clear-sky convergence profile has no peaks. The CSC paradigm, therefore, predicts no peak in cloud fraction for this experiment, but the CRM results show that the anvil peak remains in the upper troposphere (middle row of Figure 5). In the LOPEAK experiment, the clear-sky convergence peaks in the lower troposphere, which causes the CSC paradigm to predict the largest cloud fraction in the lower troposphere, coincident with the most rapid vertical variation in M. But, this is incorrect: the anvil peak remains in the upper troposphere (bottom row of Figure 5). The new framework explains the results of both experiments: the anvil clouds are not due to a peak in clear-sky convergence, but to the peak in effective cloud lifetimes in the upper troposphere. The new framework can also accurately predict cloud fraction in the DEFAULT experiment (*Text S5*, Figures S10,S11).

These results demonstrate that the increase in cloud lifetimes with altitude is what drives cloud fraction to high values in the upper troposphere of our simulations. Why, then, does cloud fraction not peak at the tropopause (e.g., Fig. 2, bottom-left), where temperatures are coldest and evaporation is most inhibited? The answer is that convective mass flux must go to zero at the tropopause, where radiative cooling goes to zero and convection is no longer needed to maintain energy balance. Therefore, in the very upper troposphere, long cloud lifetimes are in competition with declining detrainment, and the anvil peak emerges at a "sweet spot" below the tropopause where cloud lifetimes are long but there is still sufficient convective mass flux to be detrained. As the NOPEAK and LOPEAK experiments show, the height of this anvil peak does not necessarily correspond to any peak in clear-sky convergence, but emerges naturally from the competing influences of slowing cloud decay and declining convective mass flux.

7 Discussion

Are there other potential explanations for anvil clouds that we have not considered? One could argue that the high relative humidity of the upper troposphere (e.g., Romps, 2014) slows the evaporation of clouds, leading to a peak in cloud fraction there. However, Figure S4a shows that the vertical variation in RH makes only a minor contribution to the top-heaviness of mixing-induced cloud lifetimes. One might also argue that adiabatic compressional heating due to compensating subsidence evaporates clouds in the middle and lower troposphere, but is too weak in the upper troposphere to evaporate the clouds. The cloud lifetime due to subsidence heating is given by

$$\tau_{\text{subside}} = \frac{1}{w_{\text{subside}}} \left(\frac{q_{c0} - 10^{-5}}{\partial_z q_v^*} \right), \tag{15}$$

where w_{subside} is the environmental subsidence velocity. However, Figure S4b shows that τ_{subside} is more than an order of magnitude larger than τ_{new}, and so is irrelevant. Another potential explanation for anvil clouds is that cloud updrafts may slow down and bunch up as they approach the tropopause, leading to a large cloud fraction. To

the contrary, however, Figure S4c shows that the area occupied by updrafts themselves is negligible above the boundary layer.

Finally, one might attribute the long lifetime of cloud condensates in the upper troposphere not to slow evaporation, but to the radiative heating gradients within upper-tropospheric clouds, which are known to drive intra-cloud circulations (Harrop & Hartmann, 2016; Schmidt & Garrett, 2013). We tested this idea using a simulation in which clouds are rendered invisible to radiation, and found that these cloud-radiative interactions have a minor impact in our simulations (DEFAULT_CLR; *Text S1* and Figure S5). However, given the conflicting results in the literature (e.g., Boehm, Verlinde, & Ackerman, 1999; Fu, Krueger, & Liou, 1995; D. L. Hartmann, Gasparini, Berry, & Blossey, 2018), further investigation of this topic is warranted.

Taken all together, our simulations support the idea that tropical anvil cloud formation — that is, the top-heavy profile of cloud fraction that resembles a blacksmith's anvil — is fundamentally due to the slow evaporation of cloud condensates in the upper troposphere. This highlights the importance of correctly parameterizing the sinks of cloud condensates in global climate models (GCMs). Most GCMs do not account for vertically-varying cloud sinks in their computation of cloud fraction; for example, the most common type of cloud-fraction parameterization used in the combined CMIP3/CMIP5 ensemble is based on a diagnostic function of relative humidity alone (Geoffroy, Sherwood, & Fuchs, 2017; Tompkins, 2005). Recent work by Wall and Hartmann (2018) has shown that one such RH-based scheme does not reproduce the observed anvil peak in the deeply-convecting tropics of CAM5 (Neale et al., 2012). On the other hand, when applied to our simulations, RH-based schemes *would* produce an anvil peak in the upper troposphere — but not for the right reason, since we have shown that vertical variations in RH have little to do with the anvil peak.

Because anvil clouds provide potentially large climate feedbacks, the community should focus on developing parameterizations of cloud fraction that capture the physics of cloud decay. A promising starting point is the prognostic Tiedtke (1993) scheme, which includes a sink for cloud fraction that is proportional to the saturation deficit; this scheme is already in use in modified form at GFDL (Zhao et al., 2018) and elsewhere. Future work could determine whether the slow-evaporation framework we have developed here explains the anvil peak simulated by GCMs using this scheme. If decay-based schemes can capture the fundamental physics of anvil cloud formation, they might be trusted to predict changes in cloud fraction with global warming and to determine whether anvil clouds produce a positive or negative radiative feedback.

Acknowledgments

This work was supported by the U.S. Department of Energys Climate Model Development and Validation (CMDV), an Office of Science, Office of Biological and Environmental Research activity, under contract DE-AC02-05CH11231, and by the National Science Foundation under grant numbers DGE1106400 and 1535746. Numerical simulations were performed on the Cori cluster provided by the National Energy Research Scientific Computing Center, which is supported by the Office of Science of the U.S. Department of Energy under contract DE-AC0205CH11231. The cloud-resolving model DAM is documented at http://romps.org/dam/. The CRM output and run parameter files used in this manuscript are available at Zenodo (zenodo.org) under DOI 10.5281/zenodo.2372421. The authors thank Jennifer Kay for sharing cloud-fraction data from Kay and Gettelman (2009) for use in Figure 1.

References

Boehm, M. T., Verlinde, J., & Ackerman, T. P. (1999). On the maintenance of high

tropical cirrus. *Journal of Geophysical Research*, *104*, 423–433.

Bony, S., Stevens, B., Coppin, D., Becker, T., Reed, K. A., Voigt, A., & Medeiros, B. (2016). Thermodynamic control of anvil cloud amount. *Proceedings of the National Academy of Sciences*(27), 201601472. Retrieved from `http://www.pnas.org/lookup/doi/10.1073/pnas.1601472113` doi: 10.1073/pnas.1601472113

Boucher, O., Randall, D., Artaxo, P., Bretherton, C., Feingold, G., Forster, P., ... Zhan, X. Y. (2013). Clouds and Aerosols. *Climate Change 2013: The Physical Science Basis. Contribution of Working Group I to the Fifth Assessment Report of the Intergovernmental Panel on Climate Change*, 571–657. doi: 10.1017/CBO9781107415324.016

Clough, S. A., Shephard, M. W., Mlawer, E. J., Delamere, J. S., Iacono, M. J., Cady-Pereira, K., ... Brown, P. D. (2005). Atmospheric radiative transfer modeling: A summary of the AER codes. *Journal of Quantitative Spectroscopy and Radiative Transfer*, *91*(2), 233–244. doi: 10.1016/j.jqsrt.2004.05.058

Fu, Q., Krueger, S. K., & Liou, K.-N. (1995). Interactions of radiation and convection in simulated tropical cloud clusters. *Journal of the Atmospheric Sciences*, *52*(9).

Geoffroy, O., Sherwood, S., & Fuchs, D. (2017). On the role of the stratiform cloud scheme in the inter-model spread of cloud feedback. *Journal of Advances in Modeling Earth Systems*, 423–437. doi: 10.1002/2016MS000846.Received

Harrop, B. E., & Hartmann, D. L. (2012). Testing the Role of Radiation in Determining Tropical Cloud-Top Temperature. *Journal of Climate*, *25*(2007), 5731–5747. doi: 10.1175/JCLI-D-11-00445.1

Harrop, B. E., & Hartmann, D. L. (2016). The role of cloud heating within the atmosphere on the high cloud amount and top-of-atmosphere cloud radiative effect. *Journal of Advances in Modeling Earth Systems*.

Hartmann, D., & Larson, K. (2002). An important constraint on tropical cloudclimate feedback. *Geophysical Research Letters*, *29*(20), 10–13. doi: 10.1029/2002GL015835

Hartmann, D. L. (2016). Tropical anvil clouds and climate sensitivity. *Proceedings of the National Academy of Sciences*, *113*(32), 8897–8899. doi: 10.1073/pnas.1610455113

Hartmann, D. L., Gasparini, B., Berry, S. E., & Blossey, P. N. (2018). The Life Cycle and Net Radiative Effect of Tropical Anvil Clouds. *Journal of Advances in Modeling Earth Systems*, 1–31.

Hartmann, D. L., & Michelsen, M. L. (2002). No evidence for iris. *Bulletin of the American Meteorological Society*, *83*(9), 1345–1349. doi: 10.1175/1520-0477(2002)083⟨0249:NEFI⟩2.3.CO;2

Hartmann, D. L., Moy, L. a., & Fu, Q. (2001). Tropical convection and the energy balance at the top of the atmosphere. *Journal of Climate*, *14*(24), 4495–4511. doi: 10.1175/1520-0442(2001)014⟨4495:TCATEB⟩2.0.CO;2

Iacono, M. J., Delamere, J. S., Mlawer, E. J., Shephard, M. W., Clough, S. A., & Collins, W. D. (2008). Radiative forcing by long-lived greenhouse gases: Calculations with the AER radiative transfer models. *Journal of Geophysical Research Atmospheres*, *113*(13), 2–9. doi: 10.1029/2008JD009944

Kay, J. E., & Gettelman, A. (2009). Cloud influence on and response to seasonal Arctic sea ice loss. *Journal of Geophysical Research*, *114*(July), 1–18. doi: 10.1029/2009JD011773

Kessler, E. (1969). On the continuity and distribution of water substance in atmospheric circulations. *Atmospheric Research*, *38*(94), 109–145.

Krueger, S. K., Fu, Q., Liou, K. N., & Chin, H.-N. S. (1995). Improvements of an ice-phase mcrophysics parameterization for use in numerical simulations of tropical convection. *Journal of Applied Meteorology*, *34*(1).

Kuang, Z., & Hartmann, D. L. (2007, may). Testing the Fixed Anvil Tempera-

ture Hypothesis in a Cloud-Resolving Model. *Journal of Climate*, *20*(10), 2051–2057. doi: 10.1175/JCLI4124.1

Kubar, T., Hartmann, D. L., & Wood, R. (2007). Radiative and Convective Driving of Tropical High Clouds. *Journal of Climate*, *20*, 5510–5527. doi: 10.1175/2007JCLI1628.1

Li, Y., Yang, P., North, G. R., & Dessler, A. (2012). Test of the Fixed Anvil Temperature Hypothesis. *Journal of the Atmospheric Sciences*, *69*. doi: 10.1175/JAS-D-11-0158.1

Lin, B., Wielicki, B. a., Chambers, L. H., Hu, Y., & Xu, K. M. (2002). The Iris hypothesis: A negative or positive cloud feedback? *Journal of Climate*, *15*(3), 3–7. doi: 10.1175/1520-0442(2002)015⟨2713:COTIHA⟩2.0.CO;2

Lin, Y.-L., Farley, R. D., & Orville, H. D. (1983). Bulk parameterization of the snow field in a cloud model. *Journal of Climate and Applied Meteorology*, *22*.

Lindzen, R., Chou, M., & Hou, A. (2001). Does the earth have an adaptive infrared iris? *Bulletin of the American Meteorological Society*(May 1995), 417–432. Retrieved from `http://journals.ametsoc.org/doi/abs/10.1175/1520-0477(2001)082{\%}3C0417:DTEHAA{\%}3E2.3.CO;2`

Lord, S. J., Willoughby, H. E., & Piotrowicz, J. M. (1984). *Role of a Parameterized Ice-Phase Microphysics in an Axisymmetric, Nonhydrostatic Tropical Cyclone Model* (Vol. 41). doi: 10.1175/1520-0469(1984)041⟨2836:ROAPIP⟩2.0.CO;2

Mauritsen, T., & Stevens, B. (2015). Missing iris effect as a possible cause of muted hydrological change and high climate sensitivity in models. *Nature Geoscience*(April), 8–13. Retrieved from `http://www.nature.com/doifinder/10.1038/ngeo2414` doi: 10.1038/ngeo2414

Neale, R. B., Gettelman, A., Park, S., Chen, C.-c., Lauritzen, P. H., Williamson, D. L., ... Taylor, M. a. (2012). Description of the NCAR Community Atmosphere Model (CAM 5.0). NCAR Technical Notes. *Ncar/Tn-464+Str*, 214.

Romps, D. M. (2008, dec). The Dry-Entropy Budget of a Moist Atmosphere. *Journal of the Atmospheric Sciences*, *65*(12), 3779–3799. doi: 10.1175/2008JAS2679.1

Romps, D. M. (2014, oct). An Analytical Model for Tropical Relative Humidity. *Journal of Climate*, *27*(19), 7432–7449. doi: 10.1175/JCLI-D-14-00255.1

Schmidt, C. T., & Garrett, T. J. (2013). A Simple Framework for the Dynamic Response of Cirrus Clouds to Local Diabatic Radiative Heating. *Journal of the Atmospheric Sciences*, *70*, 1409–1422. doi: 10.1175/JAS-D-12-056.1

Thompson, D. W. J., Bony, S., & Li, Y. (2017). Thermodynamic constraint on the depth of the global tropospheric circulation. *Proceedings of the National Academy of Sciences*. doi: 10.1073/pnas.1620493114

Tiedtke, M. (1993). Representation of clouds in large-scale models. *Monthly Weather Review*, *121*.

Tompkins, A. M. (2005). The parametrization of cloud cover. *Moist Processes Lecture Note Series*.

Wall, C. J., & Hartmann, D. (2018). Balanced Cloud Radiative Effects Across a Range of Dynamical Conditions Over the Tropical West Paci fi c. *Geophysical Research Letters*, *5*, 1–9. doi: 10.1029/2018GL080046

Yanai, M., Esbensen, S., & Chu, J.-H. (1973). Determination of bulk properties of tropical cloud clusters from large-scale heat and moisture budgets. *Journal of the Atmospheric Sciences*, *30*.

Zelinka, M. D., & Hartmann, D. L. (2010). Why is longwave cloud feedback positive ? *Journal of Geophysical Research*, *115*(March), 1–16. doi: 10.1029/2010JD013817

Zelinka, M. D., & Hartmann, D. L. (2011). The observed sensitivity of high clouds to mean surface temperature anomalies in the tropics. *Journal of Geophysical Research: Atmospheres*, *116*(23), 1–16. doi: 10.1029/2011JD016459

Zhao, M., Golaz, J.-C., Held, I. M., Guo, H., Balaji, V., & Benson, R. (2018). The

GFDL Global Atmosphere and Land Model AM4.0/LM4.0: 2. Model Description, Sensitivity Studies, and Tuning Strategies. *Journal of Advances in Modeling Earth Systems*, *10*, 735–769. doi: 10.1002/2017MS001209